Available online at www.sciencedirect.com
SCIENCE DIRECT®
Polymer 44 (2003) 3593–3605
polymer
www.elsevier.com/locate/polymer

Mesoscale simulation of block copolymers in aqueous solution: parameterisation, micelle growth kinetics and the effect of temperature and concentration morphology

Yeng-Ming Lam[a,*], Gerhard Goldbeck-Wood[b]

[a]*Department of Materials Science and Metallurgy, University of Cambridge, Pembroke Street, Cambridge CB2 3QZ, UK*
[b]*Accelrys, 334 Cambridge Science Park, Cambridge CB4 0WN, UK*

Received 9 December 2002; received in revised form 11 March 2003; accepted 11 March 2003

Abstract

In this work, we utilise 'MesoDyn' [J Chem Phys 99 (1993) 9202; 106 (1997) 4260] density functional simulations to study the effect of temperature and concentration on the micellar morphology of polymeric surfactants. Parameterisation strategies based upon atomistic models and experimental data are discussed. Taking the temperature dependence of interaction energy into account, the change in morphology of Pluronic (PEO–PPO–PEO) block copolymer structure with temperature is well reproduced. As a function of concentration, the diameter of spherical micelles is found to increase in line with previous cryo-TEM observations [Phys Chem Chem Phys 1 (1999) 3331]. Simulations of high concentration PEO–PBO diblock systems show ordering similar to the face-centered cubic structures found experimentally [J Polym Sci B 33 (1995) 1085; Macromolecules 30 (1997) 5721; Polymer 39 (1998) 4891; Phys Chem Chem Phys 1 (1999) 2773].
© 2003 Elsevier Science Ltd. All rights reserved.

Keywords: Block copolymers; Mesoscale simulation; Micelles

1. Introduction

Block copolymers have become increasingly important in recent years due to their industrial relevance and scientific possibilities. One can 'design' a block copolymer for practically any application by synthesising different combinations of basic polymeric units. One class of block copolymer, in particular, that has gained a huge amount of interest is that of micelle forming amphiphilic polymers. They have a number of useful applications ranging from low-end non-ionic surfactants in cleaning liquids to high-end applications such as drug carriers for hydrophobic pharmaceutics. To be able to accurately predict the phases in an aqueous system using the known interaction energies of the components is very valuable, and this study is directed towards this goal.

The morphology of aqueous solutions of block copolymer can be effectively studied using the MesoDyn [1] program in Cerius2 by Accelrys. MesoDyn is based on dynamic mean field density functional theory. The phase separation dynamics is described by Langevin equations for polymer diffusion [2]. One important advantage of this method over other methods such as the self-consistent mean field theory is that there is no a priori assumption on the phases, and that the kinetics of phase formation, which is very difficult to observe experimentally, can be studied.

In the first part of this work, we elaborate on approaches to map the atomistic detail of the polymers onto the coarse-grained description used in MesoDyn. Both a simple Gaussian chain formula, and a more realistic mapping based on structure factors are put forward and compared. Interaction parameters are derived from vapour pressure data.

With parameter values derived by the above methods for amphiphilic polymers such as *Pluronic*™, (ethylene oxide) (propylene oxide) (ethylene oxide) triblock copolymers, the concentration and temperature effect on morphologies was simulated. The results are shown to compare well with experimental observations on those systems. An increase of micellar size with concentration was found, as in a previous

* Corresponding author. Present Address: School of Materials Engineering, Nanyang Technological University, Nanyang Avenue, Singapore, Singapore 639798. Tel.: +65-6790-4705; fax: +65-6790-9081.
E-mail address: ymlam@ntu.edu.sg (Y.M. Lam).

0032-3861/03/$ - see front matter © 2003 Elsevier Science Ltd. All rights reserved.
doi:10.1016/S0032-3861(03)00250-7

cryogenic transmission electron microscopy study [3]. The change of morphology from micelles to rods with increasing temperature was equally well reproduced.

Finally, simulations of high concentration PEO–PBO diblock systems show ordering similar to the face-centred cubic (FCC) structures found experimentally [4–7].

1.1. Systems studied

In this work, we study by simulation two Pluronic systems called P85 ($PO_{26}EO_{40}PO_{26}$) and F127 ($PO_{99}EO_{65}PO_{99}$), as well as a butylene oxide–ethylene oxide diblock copolymer of structure $BO_{40}EO_{10}$, which shall be called BE for short.

Micelles are usually found at a relatively low concentration compared with other phases. Depending on the type and architecture of the copolymer, and the temperature of the system, the concentration at which this structure occurs is different. For F127, the critical micellisation concentration (CMC) at about 30 °C is about 0.1 wt% [8], as measured using light scattering. The micelles are formed in a few milliseconds, and it is therefore very difficult to determine experimentally the growth rate and growth mechanism of the micelles. Using the methods outlined below, however, the micellar formation can be simulated.

2. Simulation parameterisation

To specify the chemical nature of the system in a MesoDyn simulation, two sets of parameters have to be defined: the chain topology in terms of repeat segments (or beads) and the interaction energies of the various types of segments. MesoDyn uses a Gaussian chain description with all segments of the same size. Gaussian chain statistics and structure factors of Gaussian chain block copolymers, introduced by Leibler [9] using a random phase approximation (RPA) approach, will be used in the parameterisation.

2.1. Chain topology

The chain topology depends on the degree of coarsening of the original system. For each system, there is a specific characteristic length that is related to a certain chain length of a component, similar to the Kuhn length [10]. This will give the system its chain topology. In the case of PEO–PPO–PEO triblock copolymer, the segment length will represent a certain number of monomers of PEO and a different number of PPO.

To determine the segment length, one has to compare the chain dimensions of an atomistic chain and that of a Gaussian chain. In order to obtain a statistical sample of atomistic chains we employ the RIS Metropolis Monte Carlo (RMMC) method [11], as implemented in the Cerius^2 software by Accelrys. RMMC has adjustable parameters, in particular a dielectric constant, which can be used to calibrate the method. Here we first identified the values with which the known PEO and PPO homopolymer end-to-end distances could be reproduced. For the copolymer simulations, an intermediate value weight averaged by the respective chain lengths was used. The square end-to-end distances of the three polymers found using such atomistic simulation are shown in Table 1.

Once the atomistic chain end-to-end distance is known, the appropriate Gaussian chain segment lengths are determined. There are two constraints for the definition of the chains. One of the constraints is there is only one bead size, a. So, if there are two types of monomer, we should also have beads of two types, called A and B. The segment length of A and B types, however, is restricted to be the same,

$$l(\mathrm{A}) = l(\mathrm{B}) \equiv a$$

where l(A) and l(B) refers to the length of bead A and bead B, respectively, and a refers to that common length.

The second constraint is that the end-to-end distance squared, i.e. the basic shape, of the coarsened chain and the atomistic chain should be the same

$$R_L^2(\mathrm{PEO}_N\mathrm{PPO}_M\mathrm{PEO}_N) \qquad \text{or} \qquad R_{L,0}^2 \approx R_L^2(\mathrm{A}_n\mathrm{B}_m\mathrm{A}_n)$$

where R_L refers to the end-to-end distance of the Gaussian chains, and $R_{L,0}$ refers to the end-to-end distance of the atomistic chains.

A closed formula for the bead size can now be derived if we further assume that the contour lengths of the chain in terms of monomer-size steps is equal to that of the bead chain in terms of n segment lengths. Given the fact that there is only a single bead size, we obtain

$$a \approx \frac{N}{n} l(\mathrm{PEO}) \tag{1a}$$

$$a \approx \frac{M}{m} l(\mathrm{PPO}) \tag{1b}$$

where l(PEO) and l(PPO) are the monomer sizes of EO and PO, respectively. l(PPO) and l(PBO) are estimated assuming an all *trans* conformation and the monomeric length of PEO, PPO and PBO are found to be 0.2910, 0.3394 and 0.3753 nm, respectively.

On the basis of the above assumptions, the following expression for n for both the triblock and diblock copolymers can be derived, respectively (Appendix A),

$$n^2 R_{L,0}^2 - n[2N^2 l(\mathrm{PEO})^2 + NMl(\mathrm{PPO})l(\mathrm{PEO})] = 0$$

Table 1
Sq(end-to-end distance) of different triblock copolymers

Copolymers	Sq(end-to-end distance) (nm^2)
$PEO_{26}PPO_{40}PEO_{26}$	32.4 ± 0.648
$PEO_{99}PPO_{65}PEO_{99}$	77.7 ± 2.083
$PEO_{40}PBO_{10}$	21.8 ± 0.299

Table 2
Gaussian chain approximation for various chains

Real copolymer chain	Calculated		Approximated		Gaussian chain	Averaged segment length, a (nm)
	n	m	n	M		
$PEO_{26}PPO_{40}PEO_{26}$	6.70	12.03	6	12	$A_6B_{12}A_6$	1.1960
			7	12	$A_7B_{12}A_7$	1.1061
$PEO_{99}PPO_{65}PEO_{99}$	29.54	22.62	29	22	$A_{29}B_{22}A_{29}$	0.9981
			29	23	$A_{29}B_{23}A_{29}$	0.9763
			30	22	$A_{30}B_{22}A_{30}$	0.9815
			30	23	$A_{30}B_{23}A_{30}$	0.9597
$PEO_{40}PBO_{10}$	8.23	2.65	8	2	A_8B_2	1.6658
			8	3	A_8B_3	1.3530
			9	2	A_9B_2	1.5849
			9	3	A_9B_3	1.2722

$$n^2R_{L,0}^2 - n[N^2l(\mathrm{PEO})^2 + NMl(\mathrm{PBO})l(\mathrm{PEO})] = 0$$

Therefore, if the end-to-end distance and the monomeric lengths are known, the coarsened chain topology, n and m, and the bead diameter, a, can in principle be calculated. However, since n, m have to be integer, the above equation cannot be solved exactly. There are a few approximating values in each case as shown in Table 2.

In order to confirm that this simple approach and the Gaussian chain assumption are correct, we check the above results against block copolymer structure factors and single chain scattering functions.

Firstly, using the simulated atomistic chain from 1000 independent RMMC runs, the average structure factor of P85 from the 1000 conformations is obtained (Fig. 1). The peak position yields the effective segment length of the polymer. We note that the value obtained in this way agrees well with that derived by the above arithmetic method for the case of P85.

Second, the structure factors of block-copolymers in the RPA should be a better measure of the Gaussian block-copolymer size than the simple equation. We therefore check the end-to-end distances derived above against those

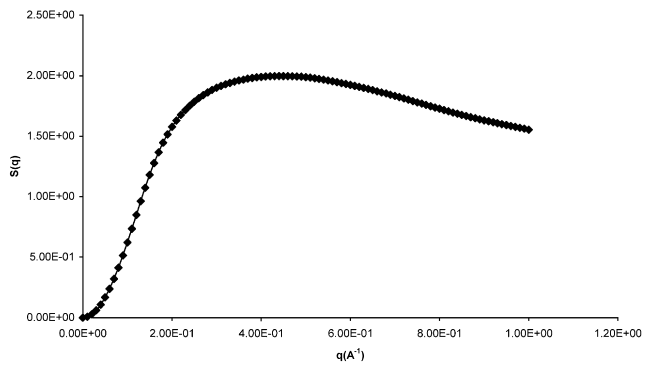

Fig. 1. Structure factor plot for $PEO_{26}PPO_{40}PEO_{26}$ as a function of scattering vector, q. The peak position corresponds to the structure factor related to the characteristic segment length associated with a certain number of monomers.

we can obtain from RPA correlation functions. The structure factor of the block copolymer is derived for the case that the monomeric interactions are turned off ($\chi = 0$), i.e. the density correlation functions are equal to that of an ideal Gaussian chain. The peak observed is due to the 'correlation hole effect' in block copolymers.[1] The resulting plot of the structure function versus scattering vector, q, is shown in this typical structure plot for the P85 copolymer with an $A_6B_{12}A_6$ structure (Fig. 2). The difference in the shape of the structure factor plot from RMMC and that calculated using RPA is due to the fact that we chose $\chi = 0$. If χ is zero, we expect a sharper negative gradient due to the absence of short-range interaction forces. However, the peak position of the correlation function of the copolymer is not dependent on the interaction parameter value, only the shape is. As shown in Appendix A, the peak of this function represents end-to-end distance, R_L.

From Table 3, the chain with architecture, $A_6B_{12}A_6$, has a chain statistics closest to that of atomistically simulated P85 chain (For the atomistic chain end-to-end distance, refer to Table 1.). This architecture is exactly the same as that derived by the arithmetic calculation earlier on.

We applied the same method to verify F127 and PEO–PBO diblock chain derived above. From the correlation function, F127 is best represented by a $A_{24}B_{20}A_{24}$ Gaussian chain and EB by a $A_{12}B_4$ Gaussian chain. (Tables 4 and 5).

For Pluronic F127 and for EB, the chain architecture differs from that deduced from the arithmetic calculation. One of the reasons may be because in the RMMC simulation, as one block of the chain gets substantially larger than the other block (such as in the case of $PEO_{99}PPO_{65}PEO_{99}$ (99×2 PEO compared to 65 PPO)), the chain is less likely to behave like a Gaussian chain under

[1] The correlation hole effect basically means that the probability of finding in the vicinity of an A monomer, another A monomer belonging to a different chain is slightly decreased due to repulsion of polymer coils. At small angles, ($q \to 0$), the scattering power goes to zero. The combined behaviour requires the presence of a maximum in the intermediate range and gives rise to the peak observed.

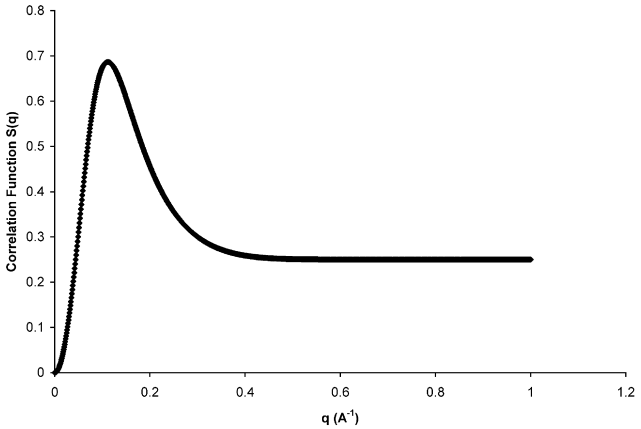

Fig. 2. Correlation function plot for $PEO_{26}PPO_{40}PEO_{26}$ derived from equations based on RPA.

the conditions imposed, which provide only for a solvent environment averaged between the PEO and PPO theta solvent conditions.

2.2. Interaction parameters

The interaction energy in MesoDyn represents the pairwise interactions of beads in a way similar to that defined in the Flory-Huggins model. It can be derived either from atomistic simulation, empirical methods [11] or from experimental data such as vapour pressure data [15] or light scattering measurements [12]. The simplest approach is based on regular solution theory and relates the Flory-Huggins χ parameter to the component solubility parameter. However, this is already an approximation for dispersive systems. The approach is not valid for polar and hydrogen bonding systems. Furthermore, effective mean–field interactions vary also with both concentration and temperature. Here we take temperature dependence into account according to

$$\chi = \alpha + \frac{\beta}{T} \tag{2}$$

Here α represents the entropic contribution. In simple terms, α is added to take into account the difference in the size of solvent and solute atoms, and β represents the enthalpic contributions. In the case of PEO and water, because of the unusual solution behaviour as mentioned earlier, the temperature dependence is particularly critical.

To define χ in a coarse grained manner, one can make use of the Flory-Huggins relationship between χ and vapour pressure which originates from the lattice model [13]. The equation which describes the interaction parameter as a function of volume fraction of polymer and its vapour pressure is

$$\chi_{IJ} = \phi^{-2}\left\{\ln\frac{p}{p^0} - \ln(1-\phi) - \left(1-\frac{1}{N}\right)\phi\right\} \tag{3}$$

where

χ_{IJ} refers to interaction parameter between component I and J,
ϕ is the volume fraction of polymer,
p^0 is the vapour pressure of pure solvent,
p is the vapour pressure of the solution, and
N is regarded as the ratio of the two molar volumes.

2.3. Determination of interaction parameters

For the interactions between polymer components and water, parameter values can be determined from experimental vapour pressure data [14] using Eq. (3). The N in the equation refers to the equivalent number of beads of the different monomer using the bead to monomer ratio described earlier. The relationship between the empirical

Table 3
Possible Gaussian architecture and its associated characteristic length and square of end-to-end distance for $PEO_{26}PPO_{40}PEO_{26}$

Copolymers	Characteristic length (nm)	Sq(end-to-end distance) (nm^2)
$A_5B_9A_5$	15.108	39.5
$A_5B_{10}A_5$	14.354	37.2
$A_6B_{11}A_6$	12.476	32.6
$A_6B_{12}A_6$	11.960	32.1
$A_7B_{12}A_7$	11.061	29.3
$A_7B_{13}A_7$	10.626	28.4

Table 4
Possible Gaussian architecture and its associated characteristic length and square of end-to-end distance for $PEO_{99}PPO_{65}PEO_{99}$

Copolymers	Characteristic length (nm)	Sq(end-to-end distance) (nm^2)
$A_{29}B_{22}A_{29}$	0.998	68.3
$A_{27}B_{20}A_{27}$	1.085	74.1
$A_{27}B_{21}A_{27}$	1.059	72.1
$A_{27}B_{22}A_{27}$	1.035	70.2
$A_{25}B_{19}A_{25}$	1.157	80.6
$A_{25}B_{20}A_{25}$	1.128	76.1
$A_{25}B_{21}A_{25}$	1.101	74.1
$A_{24}B_{18}A_{24}$	1.213	90.6
$A_{24}B_{19}A_{24}$	1.181	80.6
$A_{24}B_{20}A_{24}$	1.152	78.3

Table 5
Possible Gaussian architecture and its associated characteristic length and square of end-to-end distance for $PEO_{40}PPO_{10}$

Copolymers	Characteristic length (nm)	Sq(end-to-end distance) (nm^2)
A_8B_2	1.666	33.9
A_8B_3	1.353	29.3
$A_{10}B_3$	1.208	27.0
$A_{10}B_4$	1.051	23.7
$A_{11}B_3$	1.155	25.7
$A_{11}B_4$	0.998	22.7
$A_{12}B_3$	1.111	25.3
$A_{12}B_4$	0.954	21.7

Table 6
Interaction parameter of various molecules in solution used in simulation

Copolymer	Concentration	$\chi_{EO/Water}$	$\chi_{PO/Water}$	$\chi_{EO/PO}$	$\chi_{BO/Water}$	$\chi_{EO/BO}$
$PEO_{13}PPO_{30}PEO_{13}$	0.40–0.60	1.35	1.64	5.00	–	–
$PEO_{26}PPO_{40}PEO_{26}$	0.25–0.45	1.35	1.64	5.00	–	–
$PEO_{99}PPO_{65}PEO_{99}$	0.08–0.12	1.35	1.62	5.00	–	–
$PEO_{40}PBO_{10}$	0.80	1.40[a]	–	–	5.25[b]	5.544[c]

[a] This value is the same value taken from the vapour pressure data and the value from Venohr and co-workers [12].
[b] This value is obtained by taking the value of PBO with water to be five times that of PEO with water [24].
[c] This value is obtained by taking the value of PEO with PBO to be four times that of PEO with water [24].

Flory-Huggins parameters and the volume fraction of various homopolymers are shown in Fig. 3(a) and (b). Refer to Table 6 for the various interaction energies calculated.

For the interactions between EO and PO, we use the value as calculated by Vlimmeren and co-workers [15] using a group contribution method, which is about $\chi_{PEO/PPO} = 5$.

3. Experiments and discussions

3.1. Micellar growth

When the polymer concentration in water is higher than the CMC, micelles start to form. The micelles are first formed by chain association. The question arises as to whether the micelle growth then proceeds by polymer chain transfer between micelles or coalescence. The issue is addressed here by simulating the phase development over time.

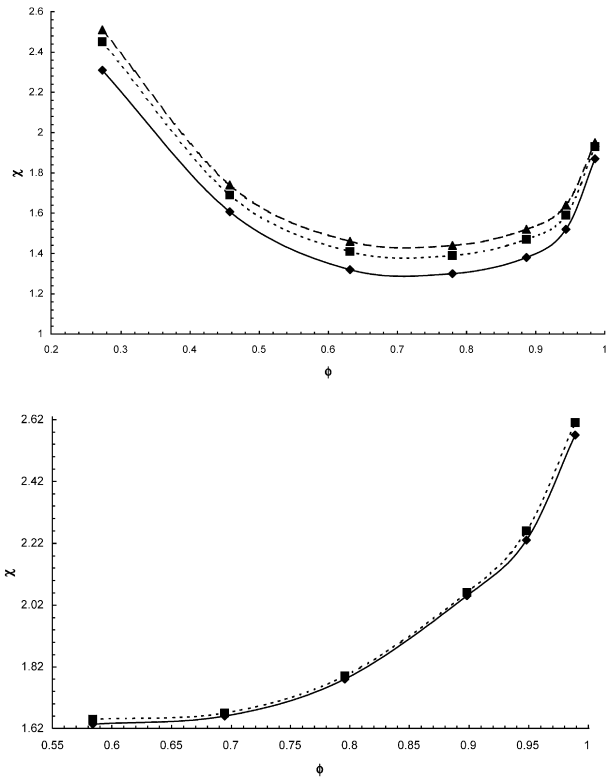

Fig. 3. Interaction parameters of PEO, PPO and water at various volume fraction, ϕ. (a) PEO300/water, (b) PPO400/Water, (–◆–) 30 °C, (–■–) 50 °C, (–▲–) 65 °C.

A set of simulations is carried out for three different block copolymers at various concentration within the micellisation range and the size of the core of the micelles is evaluated according to three criteria: the cutoff density, the circularity and the cutoff number. The cutoff density is defined as the density of beads above which the grid square will be considered as part of the micelle. As for the cutoff number, it refers to the maximum number of grid counts that will make the micelle a valid one. Both criteria are present to prevent the erroneous inclusion of a pair of coalescing micelles, hence resulting in a more accurate average.

The discretised time step of the system is dependent on the diffusion coefficient of the beads in the system, the mesh size, and the numerical scheme used to solve the density functional [16]. The value of the diffusion coefficient used is 1.0×10^{-7} cm^2 s^{-1} which is not specifically parameterised for PEO, PPO or water, but is a typical value for such a polymer system. The diffusion coefficient of poly(ethylene oxide) is about $0.9–1.3 \times 10^{-7}$ cm s^{-1} at 25 ± 0.02 °C for a relatively high molecular weight polymer and that for poly(propylene oxide) is about $1.0–1.6 \times 10^{-7}$ at about 25 °C [17]. The discretised time step found for these systems is 50 ns.

The first system that we are going to look at is a $32 \times 32 \times 32$ cube containing 24 vol% $PEO_{26}PPO_{40}PEO_{26}$, represented by a coarsened chain, $A_6B_{12}A_6$. The rest of the system is made up of water beads. The system is run for 40,000 time steps (which is equivalent to 2 ms) starting from a homogeneous system. After about 2000 time steps, micelles starts to form.

The micellar structure development may be divided into a formation and a growth stage. In the first stage of formation, micelles and monomers coexist. Hence we should expect a distribution of micelle sizes. This can clearly be seen in Fig. 4.

In the second stage, the micelles start to grow, manifested by a shift in average size towards larger radii. The micellar growth observed over time shows that the micelles grow both individually by chain transfer as well as by coalescence (Fig. 5).

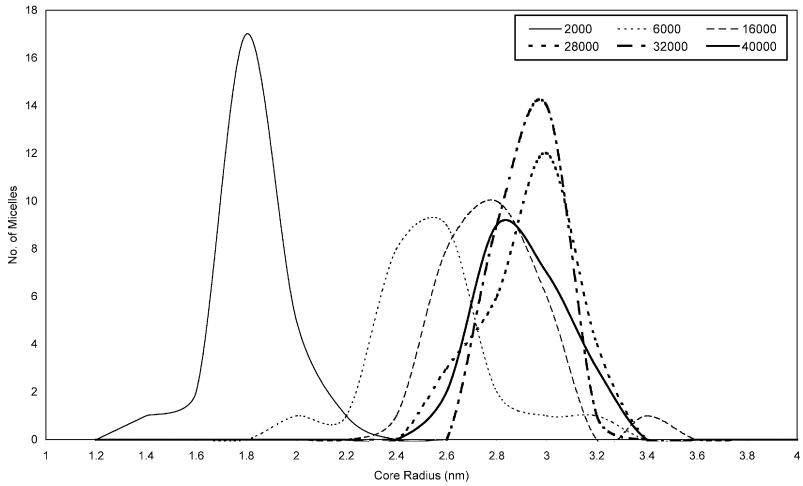

Fig. 4. Size distribution of micelles with increasing time steps. The legend in the graph gives the various time steps. Above about 10,000 time steps, the size of the micelles is rather constant just as observed in the size vs time plot.

Fig. 6 shows the order parameter as a function of time. Here, the order parameter is defined by the mean-squared deviation from homogeneity in the system, which captures the effects of phase separation. The order parameter plot in Fig. 6 shows an initial period of very little phase separation (0–2000 time steps). This resembles a nucleation stage where small aggregates are not energetically stable to grow. For times up to 10,000 time steps, the order parameter is not yet in equilibrium as the chains are still diffusing and segregating. As mentioned before, the growth of micelles during this time occurs by coalescence and chains transfer as seen in Fig. 5. In fact, looking at the growth rate of the micelles shown in Fig. 7 the gradient of the logarithmic plot of size versus time is approximately 0.30, consistent with an Ostwald Ripening behaviour.

The above observation is found over the whole micellar phase range of concentrations for this copolymer. After about 10,000 time steps, the micellar size and position remains more or less constant.

As the concentration increases, it takes a longer time for the micelles to reach their equilibrium size. The equilibrium size of the micelles for the 24% system is reached at about $0.9-1 \times 10^4$ time steps, but the equilibrium size of the micelles in the 27% system is only reached after $1.3-1.4 \times 10^4$ time steps. The reason for this difference lies in the fact that the viscosity of dilute solutions behaves hydrodynamically like a collection of solid spheres. The viscosity of the solution is directly related to the volume fraction occupied by the spheres [18]. Hence, with an increase in concentration, a longer time is required for the aggregates to diffuse towards each other to coalesce. The above micellar growth behaviour applies for all concentrations studied, i.e. 24–30 vol%.

A broadly similar behaviour was found for the other two copolymers investigated. Looking at both the order parameter and the size distribution in Fig. 8, the structures would have reached equilibrium after 6000–7000 time steps. The core radius again moves from a smaller value to a higher one with increasing time steps. The distribution of the size of the micelles is still rather wide even at 18,000 time steps. This may be due to the fact that the system has not fully equilibrated yet and should be run for longer. From the order parameter plot, there is again an initial stage of nucleation which was discussed earlier. The growth of the micelles in this system also shows a growth rate $g \propto t^{\alpha}$ with $\alpha \approx 0.3$ (Fig. 9).

The 26% aqueous solution of EB behaved similarly to the triblocks. The relationship between the radius and time in the growth region is $r \alpha t^{0.25-0.30}$.

3.2. The effect of concentration

In this section, we will see how concentration affects the morphology, firstly at low concentration where micelles are most often observed and secondly, at moderate and high concentration regions where some other phases and ordering might be observed.

3.2.1. Micellar structures

Two plots showing micellar size changes with concentration for P85 and F127 are shown in Fig. 10. The size of the micellar core in the simulated system is found to be about 2.7–3.2 nm which is similar to the value found by Mortensen and Brown [19]. There is an obvious increase in size of the cores with concentration, as observed previously by cryogenic transmission electron microscopy [3]. A reason or at least a contributing factor to this behaviour is that with an increase in the polymer concentration, the core experiences the poor solvent effect less strongly and tends not to collapse as much as in a lower concentration solution. This gives rise to a larger micellar core size. On the other hand, Mortensen and Pedersen [20], based on SANS data, deduced that the core size is independent of concentration. Mortensen and co-workers used a hard-sphere fitting for the

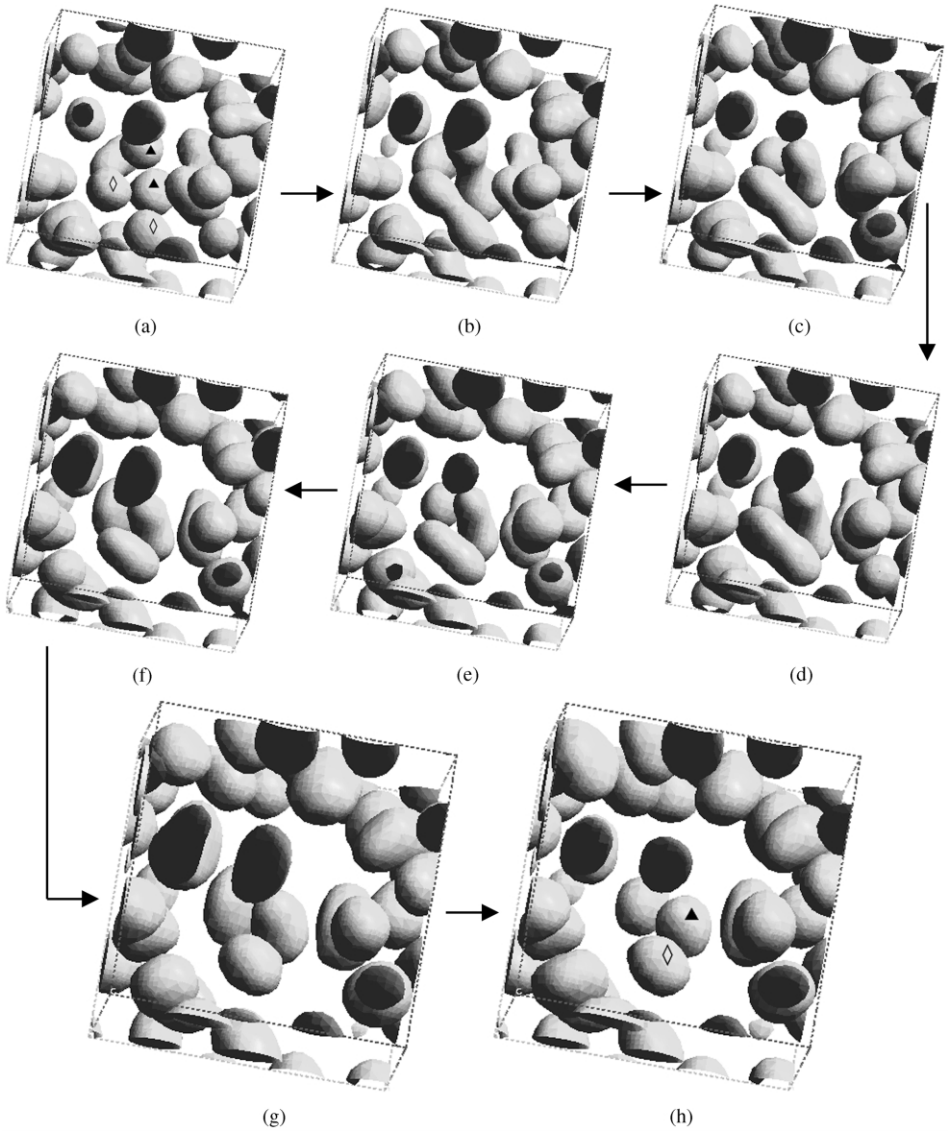

Fig. 5. Micelles of various sizes are formed due to random association with neighbouring chains. Coalescence of Micelles with increasing time steps. (a) 6500, △, ◇ micelles that coalesce, (b) 7000, (c) 7500, (d) 8000, (e) 8500, (f) 9000, (g) 9500 and (h) 10,000.

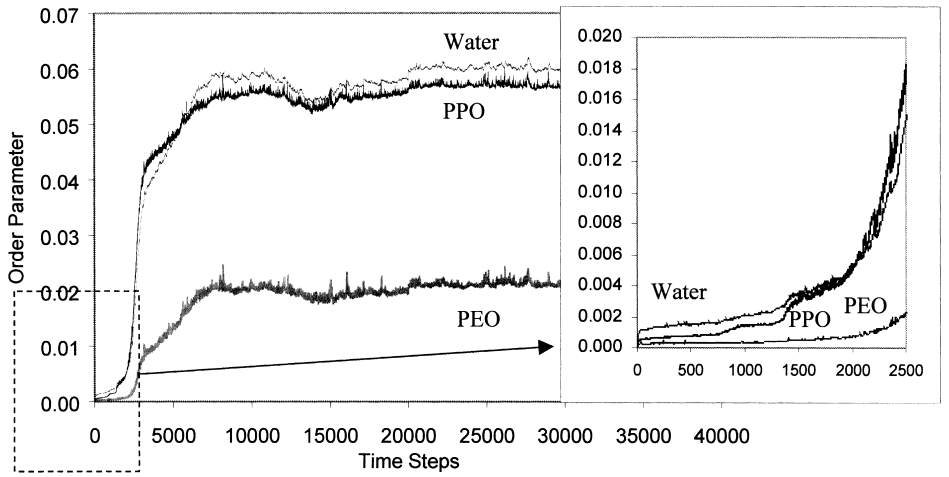

Fig. 6. Order parameter plot with increasing time for 24 vol% P85. The inset shows the exploded view of the nucleation stage.

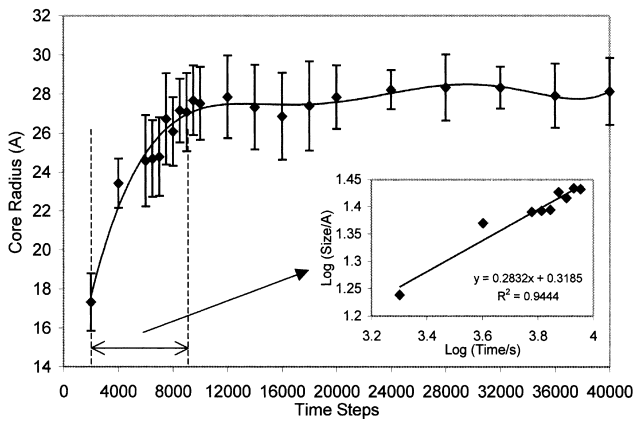

Fig. 7. Growth of core radii with time for 24 vol% $PEO_{26}PPO_{40}PEO_{26}$. At about 10,000 time steps, the core radius becomes more or less constant. The inset shows a log–log plot of the growth region.

form factor, i.e. a sharp interface between PEO and PPO is assumed. Our simulation results show that this is not the case. The discrepancy hence arises due the fact that the fitting of the SANS data ignores the dense layer of PEO at the interface between the hydrophobic core (PPO chains) and hydrophilic corona (PEO chains) [21].

(In the simulation, the size of the micelles is taken at about the middle of this interface and hence the size is sensitive to the effect of the amount of water present in the system as this affects the interaction energies between the various components. When the polymer concentration increased, there is an accompanying decrease in amount of water, hence the chains will be less collapsed and the core of the micelles increases.)

3.3. Phases observed at higher polymer concentrations

Simulations of high concentration phases of Pluronics have previously been found to give comparable morphologies to what is found experimentally [15] and we have been able to confirm these findings. With the correct parameterisation, it is possible to extend this to other similar polymer systems. Here, we therefore concentrate on aqueous solutions of EB diblock copolymers. Three concentrations of EB, 26, 40 and 60 %vol. were simulated.

Most experimental data for EB are actually performed in aqueous K_2SO_4. The reason for this is that aqueous K_2SO_4 is close to a theta solvent for the polymer. Due to the poorer solvent behaviour as compared to a pure aqueous environment, the temperature and concentration range of the phases observable in the system is effectively moved to a more convenient lower range. The effect can be seen clearly by comparing the phase diagrams of $PEO_{40}PBO_{10}$ in water and $PEO_{40}PBO_{10}$ in aqueous K_2SO_4 obtained experimentally by Deng and co-workers [4] and adapted from experiments [5, 6] by Derici and co-workers [7], respectively.

The three simulation runs show that the morphology of the aqueous systems remains micellar even to fairly high concentration. The number of micelles seen in the cube increases with concentration. We analyse the ordering by using the auto correlation function. The 3D auto-correlation describes the probability of finding another micelles at a

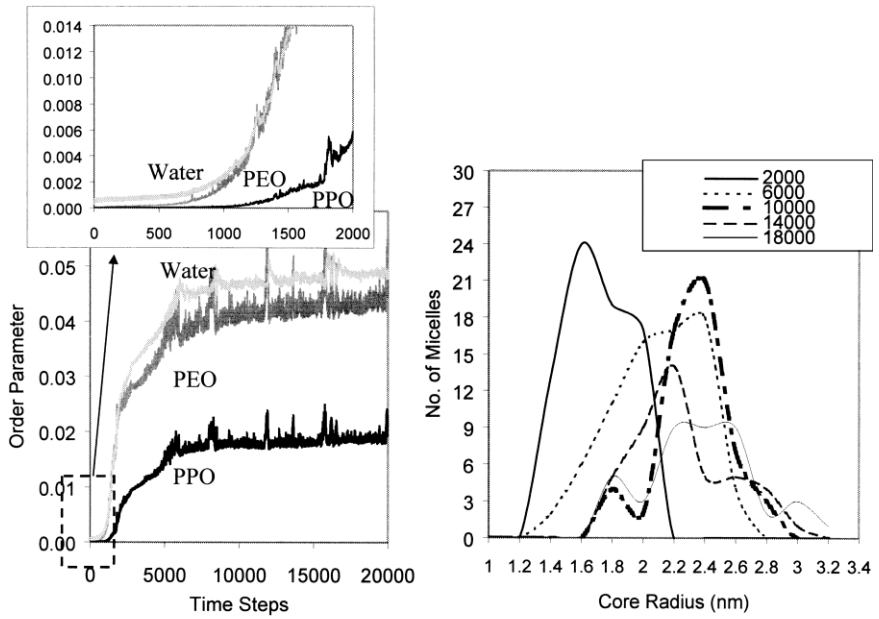

Fig. 8. (a) Order parameter plot with increasing time for 10 vol% $PEO_{99}PPO_{65}PEO_{99}$. There is an initial nucleation period (inset). (b) Size distribution with different time steps for 10 vol% $PEO_{99}PPO_{65}PEO_{99}$.

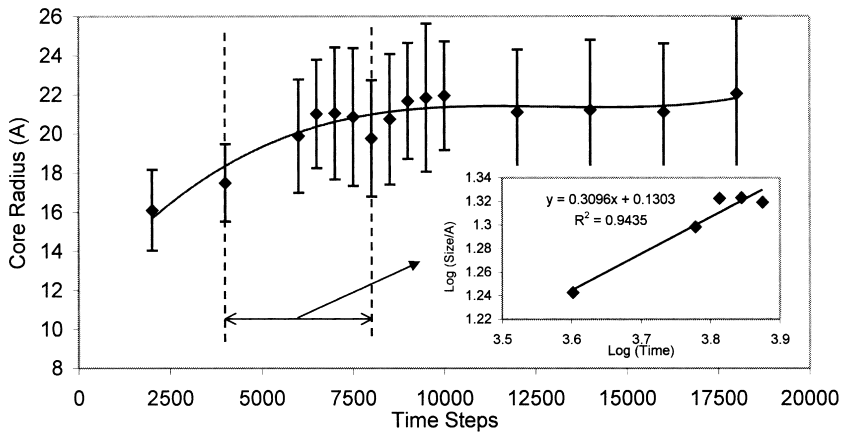

Fig. 9. Core radius plot for 10 vol% $PEO_{99}PPO_{65}PEO_{99}$ with increasing time. Inset shows that that relationship between the size of the micelles and time is give by $r \infty t^{0.30}$.

certain distance and direction from a reference micelle. What can be determined from the auto-correlation function is the symmetry of the crystal lattice and possible arrangement of the molecules or blobs [22]. The choice of using an auto correlation cube over a scattering pattern is due to the amount of noise present in the simulated structures. Reconstructions of the 3D autocorrelation cubes from the 32 slices are shown in Figs. 11 and 12.

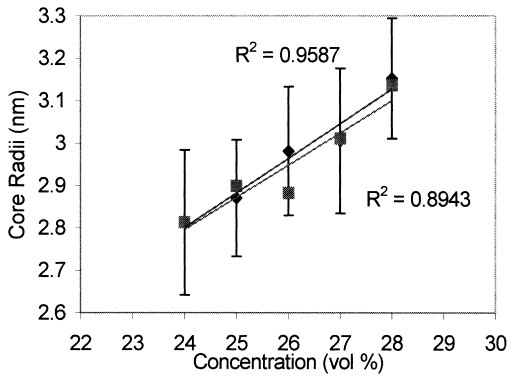

(a)

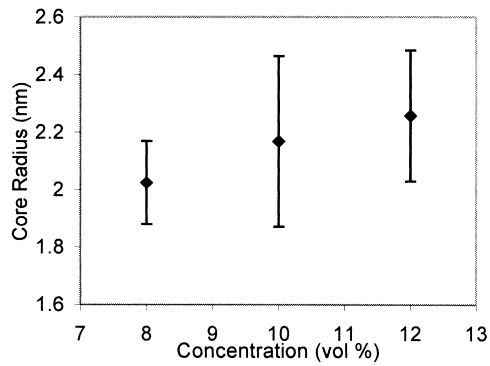

(b)

Fig. 10. Core radius of micelles dependence on concentration for (a) $PEO_{26}PPO_{40}PEO_{26}$ and (b) $PEO_{99}PPO_{65}PEO_{99}$. (■) Average last 8000 time steps; (◆) final step.

The results show an ordered structure for all three high concentrations systems. For 26 vol%. $PEO_{40}PBO_{10}$, there is an ordering on one of the planes. There is less obvious ordering out of the plane. The same happens for the 40 vol%. $PEO_{40}PBO_{10}$ (Fig. 11(a) and (b)). This is because there is an insufficient number of aggregates to determine the ordering in 3D. Looking at the two 3D autocorrelation cubes for 26 and 40 vol%. $PEO_{40}PBO_{10}$, one can start to see the ordering of the cube in the third dimension. Hence if there is a larger concentration of material, the third dimension ordering may be more obvious. On the plane where there are enough blobs, a very ordered arrangement of blobs in hexagonal packing is seen. In the 40 vol%. $PEO_{40}PBO_{10}$, the ordering is stronger as seen from the uniform blobs rather than the elongated ones in the 26 vol%. $PEO_{40}PBO_{10}$. We expect this for higher concentration systems because to pack more of these micelles into a given space, the neighbouring micelles are 'locked' in a specific position rather than having a degree of freedom in the direction that the blobs elongate.

In the 60 vol%. $PEO_{40}PBO_{10}$, there is a very obvious 3D orientation as seen in the cube. This is similar to the FCC structure. It is most obvious if we were to look down the (110) and the (111) planes in Fig. 12. In the (110) plane, there is a squashed hexagonal packing and in the (111) plane, there is a regular hexagonal packing, both of which are indicative of a FCC lattice arrangement.

As seen in the phase diagram, the high temperature phase is predominantly FCC rather than BCC. An increase in temperature tends to reduce the corona thickness and since the corona–corona interactions are attractive, this will be reduced. Hence short range intermicellar interaction will be active. This is a highly repulsive interaction. Hence one can say that short range repulsive forces favour FCC structures. This is extensively discussed in a paper by Hamley and co-workers [6] about BCC and FCC micellar arrangement in this system. At a higher concentration, as the number of

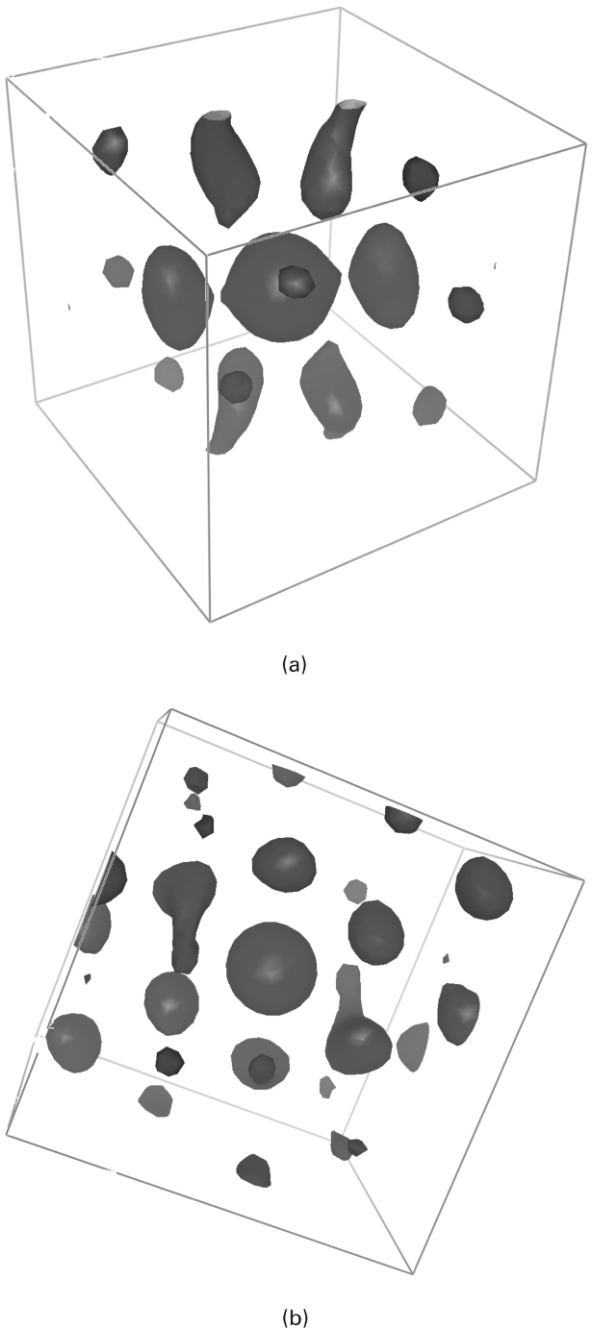

Fig. 11. 3D autocorrelation cube obtained from reconstructing from the slices. (a) 26 vol% and (b) 40 vol%.

micelles would have increased, the distance between micelles decreases and this would similarly have a strong impact on the micellar ordering.

In the simulations, there is no BCC phase at higher polymer concentrations as obtained experimentally [7]. This is because in experiments, there is a presence of SO_4^{2-} ions which promotes the formation of micelles hence increases the number of micelles in the system as compared to an aqueous system. This increase in micelles decreases the water to micelles ratio and hence the hydration level (associated OH^- ions). This may decrease the repulsive

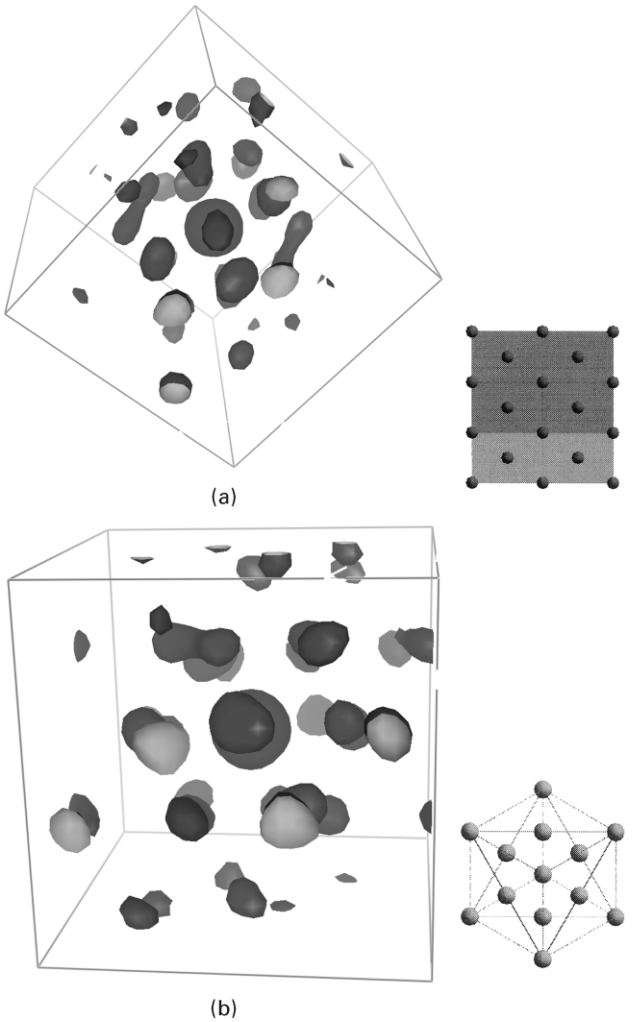

Fig. 12. 3D autocorrelation cube of the 60 vol% $PEO_{40}PBO_{10}$ obtained from reconstructing from the slices. (a) (110) plane, (b) (111) plane.

force between micelles and hence resulting in a BCC structure. In simulation, this effect is missing. Therefore, we only see the FCC structures. On top of that, the FCC structures tend to have a higher packing ratio of 0.74 than BCC (0.68). To pack a large number of micelles into the system, the system has to adopt a more efficient packing order and hence the FCC arrangement. Unfortunately, there is no high concentration data to compare the simulation with but we do know that at moderate to high concentration range, ordering is definitely present.

We have discussed the growth and the morphology of the micelles so far, and also the effect of concentration on the system. Section 3.4 will discuss briefly that the effect of a temperature can also be successfully simulated with the use of the experimental data to define the interaction parameter dependence on temperature.

3.4. The effect of temperature

Temperature has a profound effect on the phase

behaviour of triblock copolymers involving PEO and PPO due to their lower critical solution behaviour. The non-conformational entropy changes involved in this behaviour are subsumed in the mean–field interactions and must therefore be reflected by the interaction energies of the components. This section will show that the effect of temperature can be effectively reproduced if appropriate temperature dependence of the interaction energies is taken into account.

The phase diagram of Pluronic P85 ($PEO_{26}PPO_{40}$-PEO_{26}) obtained experimentally [23] by Mortensen. At a moderate temperatures, say about 40 °C, the morphology of a system containing about 30 wt% of polymer is expected to be an ordered micellar structure. At a higher temperature, 70 °C, rod-like structures are expected.

If we assumed a simple Flory-Huggins $\chi = \epsilon/kT$, the system at 70 °C would be mixed. However, if the experimental χ is taken into account (see section 2.3), the simulated morphology (Fig. 13) shows a much closer resemblance to that predicted by the phase diagram, showing rod-like regions, though the hexagonal ordering is not picked up here.

4. Conclusions

The morphological behaviour of block copolymers may be simulated with the use of dynamic mean field density functional theory via an efficient algorithm such as MesoDyn. This is because both the temporal scales and the length scales cover the time when phase transition takes place and the size of the phases observed. The growth rate of the micelle, the structure of the micelles and the effects of various factors are studied. Phases observed in experiment can be accurately reproduced.

The growth rate of the micelles is found to be rather similar to that of Ostwald ripening. The micelles grow by coalescence rather than chain transfer. The enthalpic and entropic balance of the micelles determines the equilibrium size of the micelle and it tends to take a longer time to reach in a more concentrated system.

The dependence of micellar size on concentration is found to have the same relationship as that found experimentally. That is, an increase in concentration will result in an increase in micellar size. The ordered phase found in high concentration solutions can also be reproduced using this model. In fact, in cases where interpretation of scattering results of high concentration system is difficult, the morphology can be easily determined by this simulation.

From the study of the temperature dependence of the morphology, it can be deduced that the accuracy of the prediction is strongly dependent on the accuracy of the parameterisation. The effect of the concentration and chain length on the interaction parameter should be further explored. This can be done by measuring a series of vapour pressure data of varying concentrations, temperatures and chain lengths of PEO, PPO and PBO so that the interaction parameter can be more accurately determined and hence allowing more accurate calculations of the structures at varying conditions.

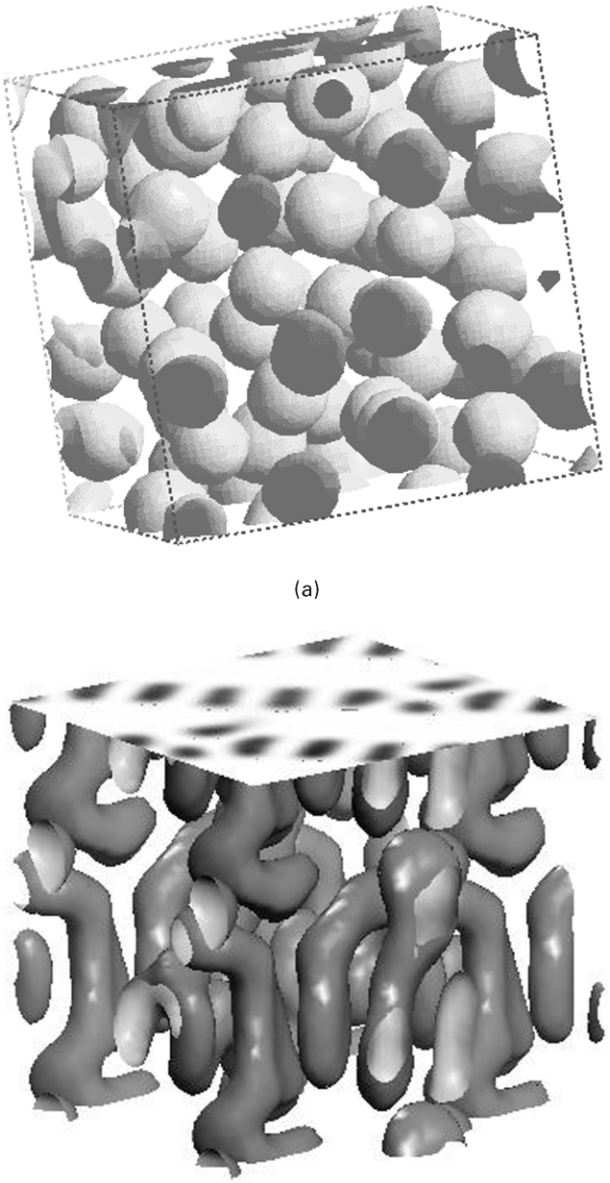

Fig. 13. Simulated morphology of 30 wt% $PEO_{26}PPO_{40}PEO_{26}$ at (a) 40 °C and (b) 70 °C.

Acknowledgements

We would like to acknowledge financial support for this work by Nanyang Technological University, Singapore.

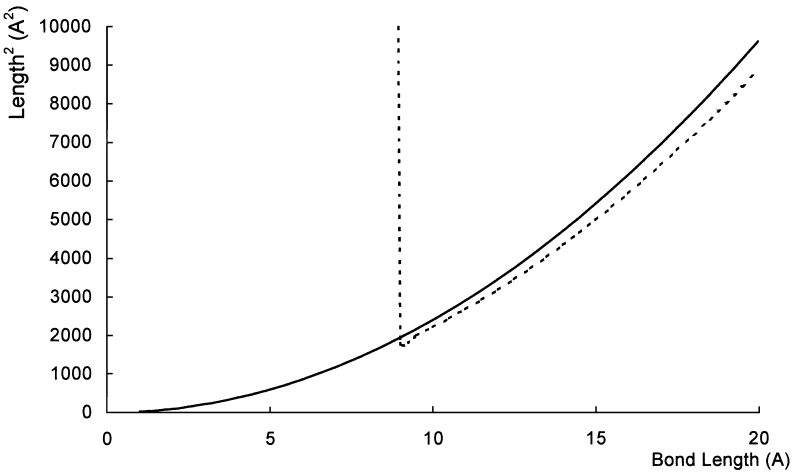

Fig. A1. Comparison of the square of the peak position with the square of end-to-end distance derived from Gaussian chain ($R^2 = Na^2$). (—) Gaussian Chain; (- - -) From correlation function.

Appendix A

A.1. Definition of the Gaussian chain

Given the constraints that there is a single bead size for PEO and PPO, the bead diameter can be defined as follows

$$a \approx \frac{N}{n} l(\mathrm{PEO}) \tag{1a}$$

$$a \approx \frac{M}{m} l(\mathrm{PPO}) \tag{1b}$$

where l(PEO) and l(PPO) refers to the length of PEO and PPO monomer, respectively. Assuming a Gaussian chain behaviour, the square end-to-end distance is defined by

$$R_L^2(\mathrm{A}_n\mathrm{B}_m\mathrm{A}_n) \approx (2n+m)a^2 = R_{L,0} \tag{A1}$$

To solve n and m, substituting Eq. (1a) into (A1),

$$(2n+m)a^2 = (2n+m)\left(\frac{N}{n} l(\mathrm{PEO})\right)^2 = \frac{(2n+m)N^2}{n^2} l(\mathrm{PEO})^2$$

$$= R_{L,0}^2$$

$$\therefore \quad (2n+m)N^2 l(\mathrm{PEO})^2 = n^2 R_{L,0}^2 \tag{A2}$$

Since from Eqs. (1a) and (1b),

$$m = \frac{M}{N}\frac{l(\mathrm{PPO})}{l(\mathrm{PEO})} n,$$

therefore Eq. (A2) becomes

$$2nN^2 l(\mathrm{PEO})^2 + \frac{M}{N}\frac{l(\mathrm{PPO})}{l(\mathrm{PEO})} N^2 l(\mathrm{PEO})^2 n - n^2 R_{L,0}^2 = 0$$

$$n^2 R_{L,0}^2 - n[2N^2 l(\mathrm{PEO})^2 + NMl(\mathrm{PPO})l(\mathrm{PEO})] = 0 \tag{A3}$$

Eq. (A3) is derived for a triblock copolymer. For diblock copolymer, the equation is as shown,

$$n^2 R_{L,0}^2 - n[N^2 l(\mathrm{PEO})^2 + NMl(\mathrm{PBO})l(\mathrm{PEO})] = 0 \tag{A4}$$

A.2. Significance of the peak in correlation function

Using the RPA definition, the correlation function plot for $\mathrm{A}_6\mathrm{B}_{12}\mathrm{A}_6$ (Gaussian chain equivalent to P85 chain) is shown in Fig. 2. The real length associated with this peak is 5.67 nm. To determine if this length represents the end-to-end distance, the peak position obtained from the derivative of $S(q)$, is plotted against the end-to-end distance.

From the comparisons in Fig. A1, it is very clear that the peak in the correlation function, $\mathrm{d}S/\mathrm{d}q = 0$, corresponds to approximately the end-to-end distance of an ideal chain at intermediate bond length. At longer segment length, we are stiffening the chain more than necessary for it to behave like an ideal chain, i.e. for the segments to be uncorrelated. At a smaller q, the same applies. Hence the comparison between the square of end-to-end distance of the calculated chain and that of an atomistic chain ($\sim 18.255 \pm 0.283\ \mathrm{nm}^2$, from Table 1) is valid.

A.2.1. Range of validity of mean field approximation

MesoDyn employs a mean field model for component interactions. This approximation is valid at concentrations greater than the overlap threshold concentration, $c^* = a^{-3}N^{-4/5}$. Here a^3 refers to the volume of a unit cell in a cubic lattice and N refers to the number of the segments that made up the polymer chain. When there is a decrease in the excluded volume in the case of a poorer solvent condition, c^* tends to increase. In our system, with the presence of hydrophilic PEO in the chains, the solvent is assumed to be close to a good solvent. One typical example is a system with P85 ($\mathrm{PEO}_{26}\mathrm{PPO}_{40}\mathrm{PEO}_{26}$) chains. Since the length of the unit cell is 1.04 nm and the Gaussian chain representing the real chain is made up of 24 segments, the overlap

threshold concentration is about $7.0 \times 10^{19}\,\mathrm{cm}^{-3}$. At a concentration of 10 vol%, the concentration of P85 chains in a $32 \times 32 \times 32$ simulation box is about $4.3 \times 10^{21}\,\mathrm{cm}^{-3}$, hence well above the overlap threshold concentration. The concentration of all the simulated systems in this paper are above the critical concentration, c^*, and hence the mean field description is reasonable.

References

[1] Fraaije JGEM. J Chem Phys 1993;99:9202–12.
[2] Fraaije JGEM, Van Vlimmeren BAC, Maurits NM, Postma M, Evers OA, Hoffmann C, Altevogt P, Goldbeck-Wood G. J Chem Phys 1997; 106:4260–9.
[3] Lam YM, Grigorieff N, Goldbeck-Wood G. Phys Chem Chem Phys 1999;1(14):3331–4.
[4] Deng N-J, Luo Y-Z, Tanodekaew S, Bingham N, Attwood D, Booth C. J Polym Sci B 1995;33:1085–96.
[5] Pople JA, Hamley IW, Fairclough JPA, Ryan AJ, Komanschek BU, Gleeson AJ, Yu G-E, Booth C. Macromolecules 1997;30:5721–8.
[6] Hamley IW, Pople JA, Fairclough JPA, Terrill NJ, Ryan AJ, Yu G-E, Booth C. Polymer 1998;39:4891–6.
[7] Derici L, Ledger S, Mai S-M, Booth C, Hamley IW, Pedersen JS. Phys Chem Chem Phys 1999;1(11):2773–85.
[8] Attwood D, Collett JH, Tait CJ. Int J Pharm 1985;26:25–33.
[9] Leibler L. Macromolecules 1980;13:1602–17.
[10] Strobl GR. The physics of polymer, 2nd ed. Berlin: Springer; 1996. Chapter 1.
[11] Honeycutt JD. Comput Theor Polym Sci 1998;8(1/2):1–8.
[12] Vehnor H, Fraajie V, Strunk H, Borchard W. Eur Polym J 1998;34(5/6):723–32.
[13] Hill TL. An introduction to statistical thermodynamics. New York: Dover Publications; 1986. Chapter 14.
[14] Malcolm GN, Rowlinson JS. Trans Faraday Soc 1957;53:921–31.
[15] Vlimmeren BAC, Marits NM, Zvelindovsky AV, Sevink GJA, Fraaije JGEM. Macromolecules 1999;32:646–56.
[16] Maurits N. PhD Thesis. Rijksuniversiteit Groningen; 1998.
[17] Brandrup J, Immergut EH. Polymer handbook. New York: Wiley; 1989.
[18] De Gennes P-G. Scaling concepts in polymer physics. Ithaca: Cornell University Press; 1979. Chapter 6.
[19] Mortensen K, Brown W. Macromolecules 1993;26:4128–35.
[20] Mortensen K, Pedersen JS. Macromolecules 1993;26:805–12.
[21] Mortensen K. J Phys: Condens Matter 1996;8:103–24.
[22] Misell DL. Image analysis, enhancement and interpretation. Amsterdam: North-Holland; 1978. Chapter 3.
[23] Mortensen K. Europhys Lett 1992;19(7):599–604.
[24] Schillen K, Claesson PM, Malmsten M, Linse P, Booth C. J Phys Chem B 1997;101:4238–52.